Journal of Hydrology 568 (2019) 174–183

Contents lists available at ScienceDirect

Journal of Hydrology

journal homepage: www.elsevier.com/locate/jhydrol

Research papers

Isotopic and geochemical assessment of the sensitivity of groundwater resources of Guam, Mariana Islands, to intra- and inter-annual variations in hydroclimate

L.K. Beal[a,*], C.I. Wong[b], K.K. Bautista[c], J.W. Jenson[c], J.L. Banner[a,b], M.A. Lander[c], S.B. Gingerich[d], J.W. Partin[e], B. Hardt[f], N.H. van Oort[g]

[a] Department of Geological Sciences, The University of Texas at Austin, Austin, TX, United States
[b] Environmental Science Institute, The University of Texas at Austin, Austin, TX, United States
[c] Water and Environmental Research Institute of the Western North Pacific, University of Guam, Mangilao, GU, United States
[d] Oregon Water Science Center, U.S. Geological Survey, Portland, OR, United States
[e] Institute for Geophysics, The University of Texas at Austin, Austin, TX, United States
[f] Earth, Atmospheric and Planetary Sciences, Massachusetts Institute of Technology, Cambridge, MA, United States
[g] Department of Earth Sciences, Utrecht University, Utrecht, Netherlands

ARTICLE INFO

This manuscript was handled by Corrado Corradini, Editor-in-Chief, with the assistance of Stephen Worthington, Associate Editor

Keywords:
Karst hydrogeology
Carbonate island aquifer
Northern Guam Lens Aquifer
Aqueous geochemistry
Oxygen isotopes ($\delta^{18}O$)
Strontium (Sr) isotopes

ABSTRACT

Assessing the sensitivity of groundwater systems to hydroclimate variability is critical to sustainable management of the water resources of Guam, US territory. We assess spatial and temporal variability of isotopic and geochemical compositions of vadose and phreatic groundwater sampled from cave drip sites and production wells, respectively, to better understand the vulnerability of the freshwater lens on Guam to variability in hydroclimate. We independently evaluate the existing conceptual model of the Northern Guam Lens Aquifer that is largely based on physical, as opposed to geochemical, observations. Sampling was conducted from 2008 to 2015, over which rainfall gradually increased. Major ion geochemistry and Sr isotope values of groundwater show varying influence from soil, limestone bedrock, and seawater. Geochemical modeling that can explain spatial variability in groundwater Na^+ and Mg^{2+} concentrations and Sr/Ca and $^{87}Sr/^{86}Sr$ values indicates that groundwater compositions are dominantly controlled by mixing of freshwater with seawater and water-rock interaction. Differences between amount-weighted annual average precipitation $\delta^{18}O$ values and groundwater $\delta^{18}O$ values indicate a recharge bias toward the wet season, consistent with other tropical carbonate island aquifer settings. Intra- and inter-annual variations in Na^+ concentrations and $\delta^{18}O$ values in groundwater reflect sensitivity of recharge to seasonal variations in rainfall amount and changes in annual rainfall amounts. Our results indicate the influence of multiple modes of recharge on groundwater compositions and spatial variability in the sensitivity of groundwater to seawater mixing. This sensitivity of the freshwater lens points to the vulnerability of groundwater resources to changes in recharge associated with climate, land-use change, and increases in population.

1. Introduction

Sustainable management of fresh groundwater resources of carbonate island aquifers is critical to the health and well-being of current and future island communities and economies. The high matrix permeability of the bedrock in carbonate systems limits surface water resources and typically makes groundwater the dominant source of potable water. Complex groundwater flow paths, dynamic interactions between the freshwater lens and underlying seawater, and changing land use and population growth can pose challenges to management of both the quantity and quality of groundwater (e.g., Chandrajith et al., 2016, Contractor and Jenson, 2000; Gingerich, 2003, 2013; Vacher and Mylroie, 2002, Rotzoll et al., 2013). Specifically, Guam's population is projected to increase from 180,000 in 2010 to 200,000 in 2020 (US Census, 2011), and expansion of the US military (SEIS, 2018) could result in an additional increase in demand on the limited freshwater

* Corresponding author at: Department of Geological Sciences, The University of Texas at Austin, 2275 Speedway, Mail Code C9000, Austin, TX 78712-1722, United States.
E-mail address: lakin.beal@utexas.edu (L.K. Beal).

https://doi.org/10.1016/j.jhydrol.2018.10.049
Received 4 May 2018; Received in revised form 17 October 2018; Accepted 19 October 2018
Available online 23 October 2018
0022-1694/ Published by Elsevier B.V.

resources of the island (Gingerich, 2013). Links between the surface and subsurface can be strong in carbonate systems, making the freshwater lens sensitive to changes in climate that affect the hydrologic cycle (e.g., Wong et al., 2012; Jocson et al., 2002; Jones and Banner, 2003). That is, the future climate may have changes in evapotranspiration, the amount, timing, or intensity of precipitation, and/or the extent of runoff and recharge (Vörösmarty et al., 2000; Allen and Ingram, 2002), yet the effects on future recharge and thus water availability of the Northern Guam Lens Aquifer (NGLA) are not well known (Gingerich, 2013). Recent model projections indicate that Guam may experience a decrease in tropical cyclone activity (Kossin et al., 2016; Park et al., 2017; Widlansky et al., in revision), and annual precipitation over the tropical Western North Pacific is projected to decrease as storm frequency and magnitude both decrease (Australian Bureau of Meteorology and CSIRO, 2011). Consequently, recharge to the NGLA would be expected to decline. Additionally, antecedent moisture conditions can significantly influence how water recharges the aquifer, especially in carbonate systems dominated by dual or triple porosities (e.g., Mahler et al., 2006; Wong et al., 2012). That is, carbonate systems can contain a combination of matrix porosity, fracture networks, and solution-enhanced fracture networks, shafts, and conduits. This range in porosity can simultaneously enable recharge through (i) slow percolation through the bedrock matrix, (ii) a relatively faster descent of a wetting front down a network of dissolution-widened fractures, and/or (iii) rapid recharge via conduits and shafts that drain dolines.

The geology and hydrogeology of the NGLA have been studied for decades (e.g., Jenson et al., 2006; Jocson et al., 2002; Mink and Vacher, 1997; Mylroie et al., 2001; Mylroie and Jenson, 2000; Tracey et al., 1964; Ward et al., 1965) yielding a conceptual model of the groundwater system that describes a transition between the freshwater lens and seawater (Gingerich, 2013). Further, critical to the conceptual model is that the NGLA is a triple-porosity aquifer, with subsurface flow through matrix pore space between carbonate sediment grains, dissolution enhanced fracture networks, and conduits (Rotzoll et al., 2013). This porosity enables rapid recharge to the aquifer, and makes recharge sensitive to antecedent moisture conditions (Contractor and Jenson, 2000; Jocson et al., 2002, Schwarz et al., 2009).

Here we present results from an isotopic and geochemical study to provide insight into the sensitivity of the freshwater lens to climate variability, and provide independent constraints on the existing conceptual model of the groundwater system, which up to now has relied on physical, as opposed to geochemical, observations and constraints. We evaluate the major cation and isotopic ($\delta^{18}O$, δD, $^{87}Sr/^{86}Sr$) compositions of vadose cave dripwater and phreatic groundwater collected during 2008–2015 to delineate the sources and processes dictating groundwater compositions and characterize the response of groundwater to changes in climate. Cave dripwater provides a unique window into Guam's thick vadose zone (60–180 m), which plays a critical role in transmitting recharge to the freshwater lens. There was a continual (monotonic) increase of rainfall from 2008 to 2015 (Supplemental Fig. S1) and the occurrence of El Niño and La Niña events enabling insight into the response of the groundwater system to inter-annual variations in rainfall amount. Our results indicate the sensitivity of recharge to both intra- and inter-annual variations in hydrologic conditions as isotopic and geochemical compositions of the freshwater lens vary in response to seasonal and inter-annual changes in precipitation amount.

2. Hydrogeologic setting

The NGLA (Fig. 1) is an eogenetic island karst aquifer, characterized by the development of porosity in young (Cenozoic) carbonates via meteoric diagenesis (Vacher and Mylroie, 2002). The aquifer has additionally been subject to post-depositional alteration and dissolution as a result of groundwater circulation. The fine-grained texture and poor sorting of the volcaniclastic basement rock that underlies the rocks of the NGLA results in much lower hydraulic conductivity than the overlying limestone bedrock (Fig. 2, Ward et al., 1965; Jocson et al., 2002). Miocene to Pleistocene marine limestone formations—the Barrigada and Mariana Limestones—occupy most of the surface of northern Guam (Tracey et al., 1964; Schlanger, 1964). The Barrigada Limestone (> 140 m thick) forms the majority of the NGLA, and consists mostly of fine-grained foraminiferal grainstone. The Mariana Limestone is comprised of reef and lagoonal sediments, and occupies the coastal periphery and most (65%) of the surface outcrop of northern Guam. It is generally coarser, more strongly cemented, and harder than the Barrigada Limestone. At the southwestern end of the limestone plateau, adjacent to the volcanic highland of southern Guam, the topmost unit is a wedge of argillaceous limestone containing fine-grained weathered volcanic sediment, and is mapped as the Hagåtña Argillaceous Member of the Mariana Limestone (Tracey et al., 1964).

Groundwater flow and storage within the NGLA is controlled by a triple-porosity system, including diffuse flow through matrix porosity (Fig. 2A and B), fracture flow through dissolution enhanced joints and fissures (Fig. 2C and D), and conduit flow in dissolution-enlarged fractures and vertical shafts draining dolines and along contacts between the limestone bedrock and volcanic basement (Jocson et al., 2002). The high inter-granular porosity of uncemented parts of the vadose zone promote high storage and infiltration via percolations along diffuse flow paths through the matrix (Fig. 2A and B). In cemented parts of vadose zone, flow is focused along enhanced fracture networks that enables faster and more concentrated percolation (Fig. 2C and D). Vacher and Mylroie (2002) showed that horizontal hydraulic conductivity in eogenetic island karst aquifers is a strong control on groundwater flow due to properties of the depositional environment and dissolution enhancement of matrix porosity at the water table. The regional hydraulic properties of the NGLA have been estimated from studies using field observations and numerical modeling to investigate the response of water levels to recharge (Jocson et al., 2002) and tidal-signal attenuation (Rotzoll et al., 2013). The Barrigada formation has estimated average matrix porosities of 0.13 and 0.21 above and below the water table, respectively, and groundwater flow largely occurs through secondary porosity (K > 12,000 m/day), whereas the hydraulic conductivity of the Mariana Limestone is approximately 730 m/day with an average porosity of 0.13 (Rotzoll et al., 2013).

There are three groundwater zones within the NGLA: the basal, para-basal, and supra-basal zones (Gingerich, 2013) (Fig. 1). The freshwater lens in the basal groundwater zone is thin, occurs entirely within the limestone units, and is underlain by seawater. The freshwater lens in the para-basal zone is in contact with the underlying volcanic unit and, as a result, is less vulnerable to mixing with seawater. Groundwater in the supra-basal zone is underlain by volcanic basement and stands above mean sea level, and is, therefore, completely isolated from seawater.

Intra- and inter-annual variations in the thickness of the freshwater lens (e.g. storage) are influenced by the amount of recharge and withdrawal (Jocson et al., 2002; Gingerich, 2013). Guam has a tropical wet-dry climate with stable temperatures year-round and a mean annual rainfall of ~2.4 m, about 70% of which falls in the wet season from June to December (Supplemental Fig. S2). Recharge to the aquifer is estimated to be 50% of mean annual rainfall, but may vary locally from 40% to 60% (Johnson, 2012). Highest recharge rates occur in areas that receive runoff from storm drain systems, whereas the lowest recharge rates occur in urban areas where storm water runoff is routed to the ocean (Johnson, 2012). Additions to groundwater recharge occur in urban areas of northern Guam through irrigation, septic leachate, and water main pipe leakage (Johnson, 2012). Antecedent moisture conditions also play a role in transmission of recharge to the freshwater lens. Recharge may take several months to percolate to the lens under dry conditions, in contrast to rapid (hours to days) transmission of recharge under wet conditions or during high-intensity rain events (Contractor and Jenson, 2000; Jocson et al., 2002). Slower recharge

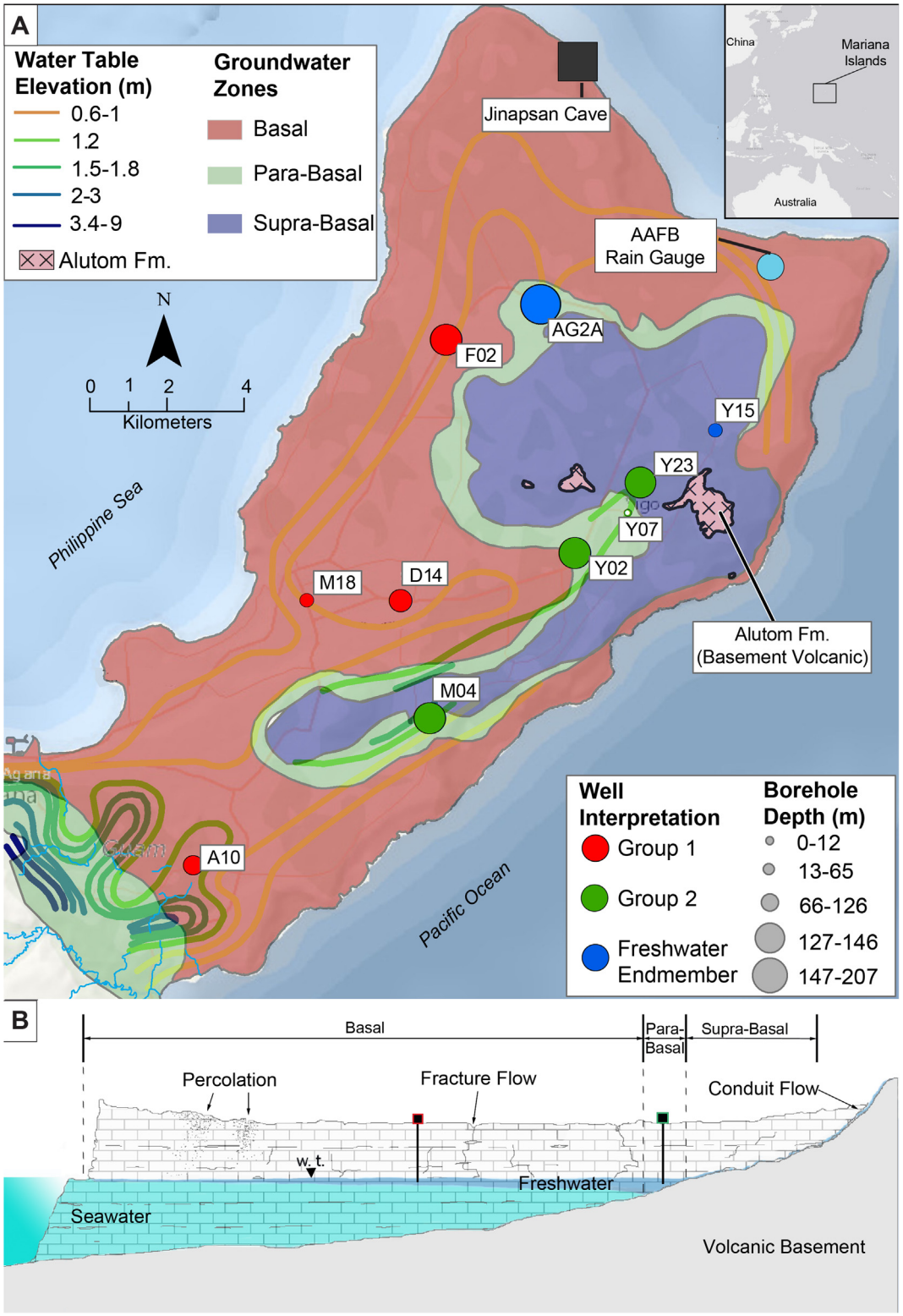

Fig. 1. (A) Map of the groundwater zones of the NGLA, and sampled wells with size and color of the symbols reflecting depth and geochemical interpretations. Inset map (upper right) to reference location of Mariana Islands, in which Guam is located. (B) Composite cross-section (not to scale) depicting wells accessing basal (red), and para-basal (green) groundwater zones. Figure modified from Vann et al. (2014). The base map and potentiometric lines were obtained from ESRI (accessed July, 2017), and the Digital Atlas of Northern Guam (acces July, 2017), respectively. (For interpretation of the references to color in this figure legend, the reader is referred to the web version of this article.)

rates under drier conditions likely reflects vertical propagation along a fine, fracture network, as opposed to direct recharge along discrete, solution widened conduits that likely facilitates high hydraulic conductivity estimated from regional-scale groundwater flow path studies. Furthermore, inter-annual variations in precipitation amount are sensitive to the El Niño - Southern Oscillation (ENSO), with wetter years corresponding to El Niño events (Guard et al., 2009), and drier years, corresponding to La Niña events or the year following an El Niño event

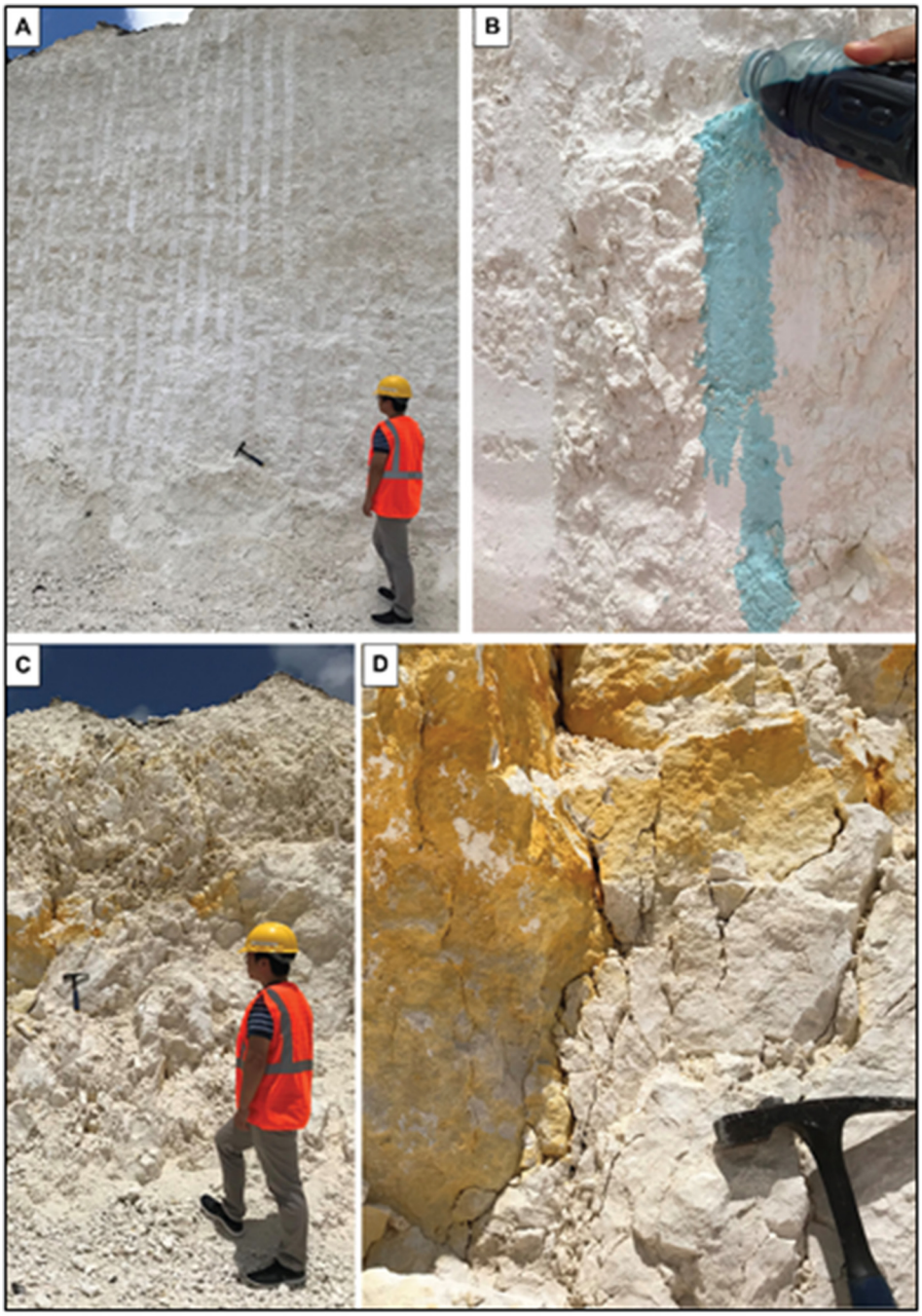

Fig. 2. Images of the Barrigada Limestone showing the poorly cemented, unfractured zone (A and B) and the cemented, coarsely friable, and fractured zone (C and D) taken at the Dededo Public Works Quarry, Guam. Rapid absorption is demonstrated with blue-colored water in (B). Staining shown in (D) is attributed to frequent percolation by vadose water carrying iron-rick minerals originating in soil. (For interpretation of the references to color in this figure legend, the reader is referred to the web version of this article.)

(Lander, 1994a,b).

3. Methods

Rainwater and groundwater from the vadose and phreatic zones were monitored over eight years (Partin et al., 2011; Noronha et al., 2016; Bautista et al., 2018). Rainfall was sampled every two weeks and cave dripwater was sampled every 4–6 weeks during 2008–2015, which spanned La Niña and El Niño conditions (Supplemental Table S1). Groundwater from the NGLA was sampled quarterly from 10 wells from mid-2013 through 2015. The wells selected for this study are representative of the groundwater compositions for the three groundwater zones (Fig. 1), and span the six hydrologically connected groundwater basins that make up the NGLA (delineated by the Guam Environmental Protection Agency). Cave dripwater was collected at five sites (ST1, ST2, SMP, FTM, and TRN) within Jinapsan Cave that we hypothesize to represent water from dominantly diffuse (ST2 and SMP) and dominantly fracture flow paths (ST1, FTM, and TRN) based on their physical, isotopic, and geochemical properties. This study draws on existing cave drip rate and cave dripwater $\delta^{18}O$ and cation (Ca concentrations and Mg/Ca and Sr/Ca values) data presented in Partin et al. (2011) and Noronha et al. (2016), which both focused on understanding how cave mineral deposits (speleothems) can be used to reconstruct past climate. This manuscript integrates existing cave

dripwater data with previously unreported cave dripwater geochemical data (Na^+ and Mg^{2+} concentrations) and geochemical and isotopic data on phreatic groundwater compositions to investigate groundwater recharge processes. It should be noted that (i) the vadose zone above the cave is a few meters thick, whereas the thickness of the vadose zone over the wells is well over 100 m, and (ii) the cave is formed in Mariana Limestone, which is well-cemented compared to the well lithified to extremely friable Barrigada Limestone (Tracey et al., 1964) in which the 10 sampled wells were completed. Fractures are visible in the cave ceiling, and the more rapidly-dripping sites in the cave are associated with them (Bautista et al., 2018). Water samples were collected in pre-cleaned HDPE Nalgene bottles, and wells were sampled using plastic submersible bailers. The water samples were decanted into pre-cleaned glass vials with no head space for stable isotope ($\delta^{18}O$ and δD) analysis and acid-cleaned HDPE plastic vials for analysis of cation concentrations and Sr-isotope ($^{87}Sr/^{86}Sr$) compositions. Well-water samples were filtered using a pre-cleaned 0.45-micron syringe filtration in the field. Samples analyzed for cation concentrations and $^{87}Sr/^{86}Sr$ values were acidified with concentrated ultrapure HNO_3.

Cation concentrations were determined using Quadrupole Inductively Coupled Plasma (ICP)-Mass Spectrometry and the ICP Optical Emission Spectrometry in the Department of Geoscience at the University of Texas at Austin (UT). The Quadrupole ICP-Mass Spectrometry analytical uncertainty for Sr^{2+}, Na^+, Ca^{2+}, Mg^{2+} is 0.04×10^{-2}, 0.02, 0.03, and 0.02 ppm, respectively, based on two times the standard error of replicate analyses of the internal standard. The ICP Optical Emission Spectrometry analytical uncertainty for Sr^{2+}, Na^+, Ca^{2+}, Mg^{2+} is 0.04×10^{-2}, 1.19, 1.91, and 0.36 ppm, respectively, based on two times the standard error of replicate analyses of the internal standard. The median percent difference between replicate analyses of samples collected at the same place and time (n = 99) for the Sr^{2+}, Na^+, Ca^{2+}, Mg^{2+} was 2.9%, 4.3%, 4.9%, and 5.6%, respectively (Supplemental Table S2). Detection limits for Sr^{2+}, Na^+, Ca^{2+}, Mg^{2+} (0.01, 1.47, 1.95, 0.29 ppb, respectively) are well below the elemental concentrations measured in unknown samples (Supplemental Table S2). Waters were analyzed for stable isotope (δD and $\delta^{18}O$) compositions using a Thermo Scientific Delta V Isotope Ratio Mass Spectrometer (IRMS) equipped with a GasBench sample introduction system and Picarro L2130-i at the UT. Uncertainty, based on two times the standard error of replicate analyses of internal standards, is ± 8‰ for δD and ± 0.2‰ for $\delta^{18}O$ for the IRMS and ± 1‰ for δD and ± 0.1‰ for $\delta^{18}O$ for the Picarro. Water isotopic measurements are reported in ‰ VSMOW. The mean difference between replicate analyses of δD (n = 31) and $\delta^{18}O$ (n = 62) was 5.8‰ and 0.3‰, respectively. Stable isotope data were also retrieved from the Global Network of Isotopes in Precipitation (GNIP; IAEA/WMO, 2018). $^{87}Sr/^{86}Sr$ values of groundwater and leachates from surficial soil and saprolite samples were determined following the methods of Musgrove and Banner (2004) using a Thermo Triton Thermal Ionizing Mass Spectrometer (TIMS) at UT. The mean $^{87}Sr/^{86}Sr$ value for the standard NBS-987 was 0.71025 ± 0.000016 (n = 30). Blank values were negligible (7 pg of Sr^{2+}) with respect to sample size (200 ng). $^{87}Sr/^{86}Sr$ values used for the limestone bedrock are estimated based on secular seawater $^{87}Sr/^{86}Sr$ curve (Hodell et al., 1991, McArthur et al., 2006, Eidvin et al., 2014; $^{87}Sr/^{86}Sr$ = 0.7088–0.7091), assuming that the limestone Sr isotope compositions have experienced negligible alteration by diagenesis. $^{87}Sr/^{86}Sr$ values for the volcanic bedrock values were obtained from Hickey-Varags and Reagan (1987, 87Sr/86Sr = 0.7035–0.7038). Daily precipitation data were retrieved from the Guam Naval Air Station/Weather Forecast Office (NAS/WFO), the NOAA Weather Service Meteorological Observatory (WSMO), and Andersen Air Force Base (AAFB). AAFB and NAS/WFO are available from the National Climate Data Center, stations as “PGUA” and “PGUM”, respectively.

The evolution of dripwater Sr/Ca and $^{87}Sr/^{86}Sr$ values due to water-rock interaction is modeled following Banner and Hanson (1990). Here we consider water-rock interaction to include recrystallization of calcite. Iterative mass balance calculations simulate increments of water passing through a given volume of bedrock (measured in moles), assuming each increment of water comes to elemental and isotopic equilibrium with the bedrock. These equilibrium values are calculated using the K_D value of Sr incorporation into calcite of 0.057 (Sinclair et al., 2012). The initial dripwater Sr/Ca value (0.2) were assigned based on the lowest dripwater Sr/Ca measured at each cave (Fig. 5). That is, the lowest dripwater Sr/Ca values represent the least evolved waters via water-rock interaction. Initial dripwater $^{87}Sr/^{86}Sr$ values were assumed to have the median $^{87}Sr/^{86}Sr$ value (0.709107) from measurements of soil leachates (e.g., Banner et al., 1996; Musgrove and Banner, 2004; Wong et al., 2011; Wortham et al., 2017). Two sets of water-rock interaction trends are calculated for each cave system using the highest (0.7091; Fig. 5 Water-Rock Interaction I) and lowest (0.7088; Fig. 5 Water-Rock Interaction II) bedrock $^{87}Sr/^{86}Sr$ values estimated from the seawater Sr isotope curve (Hodell et al., 1991, McArthur et al., 2006, Eidvin et al., 2014) and stoichiometric Ca (400,000 ppm) and a Sr concentration of 160 ppm (Schlanger, 1964). These two curves constrain the range of possible dripwater values that could evolve under water-rock interaction. The varying isotopic composition throughout the Barrigada Limestone (> 140 m) is constrained to maximum (i.e. younger) and minimum (i.e. older) $^{87}Sr/^{86}Sr$ values (0.7091 and 0.7088, respectively) used in the model. In addition to the water-rock interaction model, fluid mixing is calculated between groundwater and seawater (Fig. 5 dashed curve). The groundwater endmember is represented by the average Sr/Ca and $^{87}Sr/^{86}Sr$ values from wells with extensive water-rock interaction (Y23, Y15, Y07, and Y02), and the seawater endmember has Sr/Ca and $^{87}Sr/^{86}Sr$ values of 8.9 (Turekian, 1968) and 0.70918, respectively.

4. Results and discussion

4.1. Delineating controls on phreatic groundwater compositions

Groundwater geochemical compositions are spatially variable, especially with respect to Mg^{2+} and Na^+ concentrations (Fig. 3). Three end-member compositions were identified, (i) low Na^+ and Mg^{2+} concentrations (AG2A, and Y15, herein freshwater end member), (ii) high Na^+ and Mg^{2+} concentrations, and (iii) low Na^+ and high Mg^{2+} concentrations (Fig. 3). One group of groundwater compositions is consistent with variable mixing (up to 1%) between the freshwater end member and seawater (Wells A10, F02, D14, and M18; referred to herein as Group 1). Another group of groundwater compositions deviates from the mixing line with elevated Mg^{2+} concentrations (Wells Y23, Y02, Y07, and M04; referred to herein as Group 2) (Fig. 3). Elevated Mg^{2+} concentrations in Group 2 might result from the interaction of infiltrating meteoric water with the carbonate bedrock. That is, water can interact with the bedrock via dissolution or recrystallization of the bedrock. Group 1 wells tend to be located to the north and/or west of Group 2 wells, and are within the basal zone (Fig. 1). Geochemistry of Group 1 groundwater indicates mixing between freshwater and seawater is a dominant control on groundwater compositions (Fig. 3), and is consistent with the description of the basal zone as where the freshwater lens is thin and underlain by seawater (Fig. 1). Group 2 wells occur within the para-basal and supra-basal zones where the extent to which the freshwater lens is underlain by seawater, and hence susceptible to mixing, is limited.

Groundwater Na^+ concentrations exhibit limited temporal variability, with variations barely exceeding analytical uncertainty (Fig. 4). At several wells, however, subtle variations are evident. For example, Wells A10 and Y15 have relatively low concentrations during the wet season (159 and 8.41 ppm, respectively) relative to the dry season (186 and 10.3 ppm, respectively). This indicates some dilution of Na^+ concentrations due to recharging rainwater reaching the freshwater lens. Additionally, several of the wells with low Na^+ concentrations (< 20 mg/L; Wells AG2A, Y23, Y02, and M04) exhibit statistically

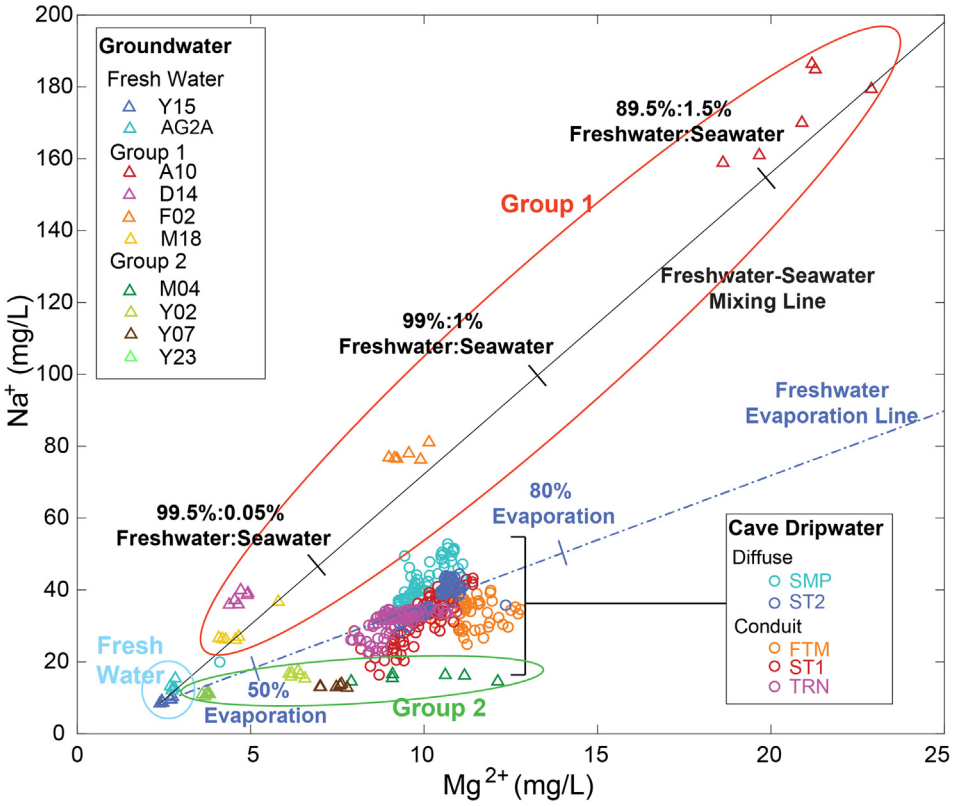

Fig. 3. Bivariate plot of cave dripwater and groundwater Mg^{2+} and Na^{+} concentrations with model curve of freshwater-seawater mixing and evapo-concentration of freshwater. Freshwater represented by groundwater with lowest Na^{+} (8.4 ppm) and Mg^{2+} (2.4 ppm) concentrations. Seawater represented by Na^{+} and Mg^{2+} concentrations of 10,800 and 1290 ppm, respectively (Turekian, 1968).

significant decreasing trends in concentrations over the study period (Supplemental Table S6), which is coincident with the continual increase of rainfall over the study period 2013–2015 (Fig. 4 and Supplemental Fig. S1). Decreasing Na^{+} concentrations at these sites indicate that the freshwater lens, in places, is sensitive to inter-annual variations in recharge. The occurrence of limited variations in Na^{+} concentrations on intra- and inter-annual time scales indicates the sensitivity of parts of the aquifer system to changes in hydrologic conditions. The limited magnitude of variation in geochemical compositions, however, reflects the ability of water in storage to buffer water compositions to large changes in hydrologic conditions (e.g., transitions between wet to dry seasons). It is pertinent, however, that there were no storms during the study period of sufficient intensity to induce ponding in dissolution dolines or otherwise activate regional-scale conduit flow other than Typhoon Dolphin (May 2015) that only grazed the northern tip of the island.

Geochemical modeling of the evolution of the isotopic and geochemical compositions of groundwater can explain most groundwater Sr/Ca and $^{87}Sr/^{86}Sr$ values (Fig. 5). Infiltrating water initially acquires a $^{87}Sr/^{86}Sr$ value from the soil that tends to be higher than that of the underlying marine carbonate bedrock (0.7088–0.7091) (Fig. 5 inset). The $^{87}Sr/^{86}Sr$ value of infiltrating water gradually evolves via water-rock interaction to lower values that are more similar to that of the bedrock.

In this process, water dissolves marine carbonates with higher Sr concentrations relative to the Sr concentrations in the calcite that is re-precipitated, thereby increasing the Sr/Ca value in the infiltrating water as the $^{87}Sr/^{86}Sr$ value is shifted toward that of the bedrock (e.g. water-rock interaction curves in Fig. 5; Banner et al., 1996; Musgrove and Banner, 2004; Wong et al., 2011; Wortham et al., 2017). Our model is constrained by measured values for soils and assumes values for the carbonate bedrock based on the age range of the Barrigada Limestone and the corresponding range of values from the reconstructed temporal variability in marine Sr-isotope values (Hodell et al., 1991, McArthur et al., 2006, Eidvin et al., 2014).

The large spread in possible bedrock values results in a large range of Sr/Ca and $^{87}Sr/^{86}Sr$ values to be accounted for by water-rock interaction, and, indeed, all but one of the groundwater compositions can be explained by this modeling effort (i.e., groundwater compositions in Fig. 5 fall between the two water-rock interaction curves). We do note that the Sr/Ca and $^{87}Sr/^{86}Sr$ values from wells Y15, Y02, Y07, Y23 create a trend that parallels one of the water-rock interaction curves (Water-Rock Interaction II in Fig. 5), potentially reflecting the evolution of groundwater compositions via water-rock interaction with bedrock with similar $^{87}Sr/^{86}Sr$ values that are close to 0.7088. Importantly, these wells have Na^{+} and Mg^{2+} concentrations that indicate groundwater is not mixing with seawater at these locations in contrast to Group 1 wells (Fig. 3). Interestingly, Group 1 Sr/Ca and $^{87}Sr/^{86}Sr$ values do align with a mixing curve between the well interpreted as Freshwater (Y15) and seawater (Fig. 5). This supports the hypothesis that Group 1 groundwater compositions are dominantly influenced by seawater mixing with freshwater that has undergone water-rock interaction. Sr/Ca and $^{87}Sr/^{86}Sr$ values of M04 do not align with the rest of Group 2 compositions, and, instead, fall along the seawater-mixing curve in Fig. 5. This, however, is inconsistent with Na^{+} and Mg^{2+} concentrations that do not reflect seawater mixing (Fig. 3). M04 is spatially distinct from the other Group 2 wells, so the Sr/Ca and $^{87}Sr/^{86}Sr$ values that are distinct from other Group 2 wells might reflect water-rock interaction with bedrock of a different $^{87}Sr/^{86}Sr$ value.

4.2. A view of recharge from the vadose zone

Cave dripwater Mg^{2+} and Na^{+} concentrations are distinct relative to those of groundwater. Na^{+} concentrations of dripwater are elevated relative to those of Group 2, but Na^{+} and Mg^{2+} concentrations do not align with the freshwater-seawater mixing curve as do those of Group 1 well waters (Fig. 3). The inability of the freshwater-seawater mixing curve to account for the dripwater indicates that cave dripwater compositions are likely not strongly influenced by sea spray despite the proximity of the cave to the ocean. Both the Barrigada and Mariana

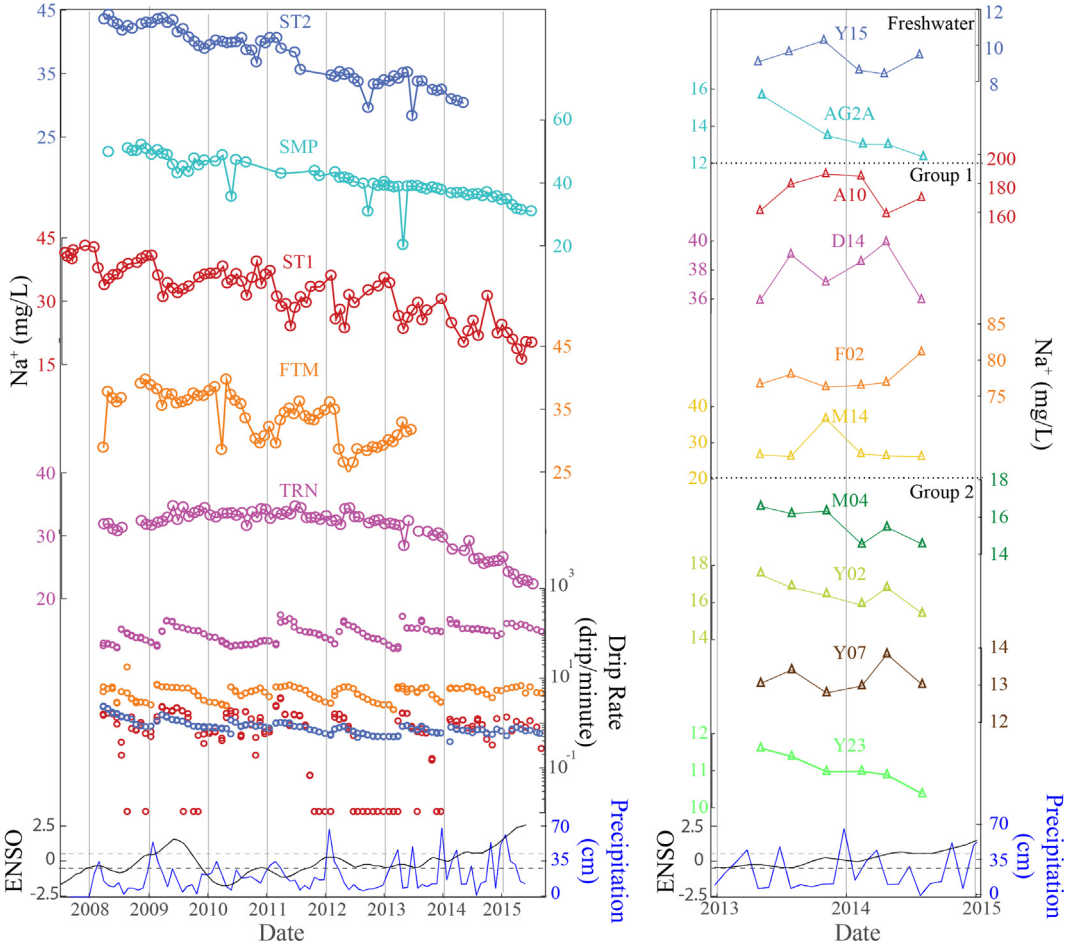

Fig. 4. Time series of cave dripwater (left panel) and groundwater (right panel) Na^+ concentrations with cave drip rate, monthly precipitation (blue), and the El Niño Southern Oscillation 3.4 Index (black). Intra- and inter-annual variations in Na^+ concentrations are more pronounced at dripwater sites relative to groundwater wells. (For interpretation of the references to color in this figure legend, the reader is referred to the web version of this article.)

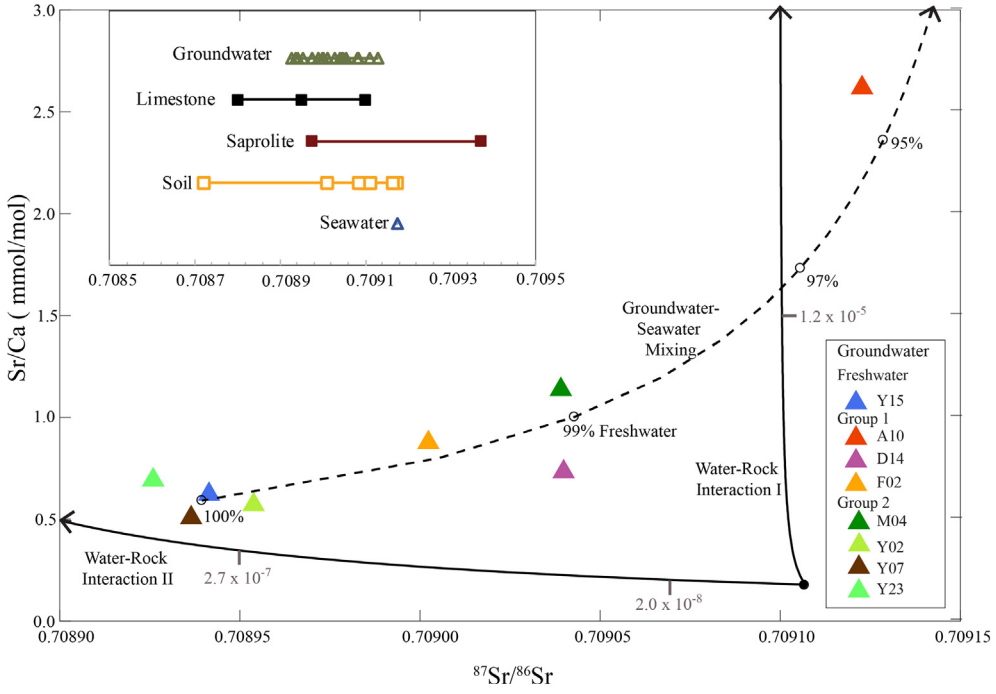

Fig. 5. Measured groundwater Sr/Ca and $^{87}Sr/^{86}Sr$ values with modeled (solid curves) evolution of groundwater compositions via water-rock interaction from an initial composition (solid black circle). The inset graph represents the range of $^{87}Sr/^{86}Sr$ values for the study area measured as a part of this study (groundwater, saprolite, and soil) and retrieved from the literature (seawater and bedrock). Fluid-rock ratios (molar) are given along the curves (grey ticks). Mixing between groundwater and seawater is also shown (dashed curve). See *Methods* for discussion of modeled curves.

Limestone Formations are high energy, reef-type settings in which deposition of evaporates was limited (Tracey et al., 1964), making the bedrock an unlikely source of Na^+. Variations, however, in cave dripwater Mg^{2+} and Na^+ concentrations can be accounted for by evapoconcentration of freshwater (Freshwater Evaporation line in Fig. 3). Cave dripwater δD and $\delta^{18}O$ values fall on the Global Meteoric Water Line (GMWL) suggesting negligible influence of evaporation on the water isotopic compositions (Supplemental Fig. S3). Combined, these results indicate that water reaching the cave has undergone little evaporation, although the water infiltrating the cave is likely carrying salts precipitated from freshwater that previously evaporated. That is, rainfall that does not recharge the cave likely evaporates in the soil, epikarst, or shallow vadose zone, leaving behind salts that are later flushed into the cave during recharge intervals.

Seasonal variability in Na^+ concentrations is evident at two of the sites dominantly supplied by fracture flow (ST1 and FTM) (Fig. 4). Lower concentrations follow the wet season at these two sites, indicating the dilution of Na^+ concentrations of water stored in the vadose zone by infiltrating meteoric water, which is consistent with seasonal increases in drip rate. The presence of seasonal variability at some sites and absence at the other cave drip sites highlights the presence of distinct recharge pathways – diffuse pathways that drain the more homogenous and geochemically invariant water in storage in the vadose zone (Fig. 2A and B) (e.g. Moerman et al., 2014) and flow along dissolution enhanced fracture networks (Fig. 2C and D) that can by-pass much of the water stored in the vadose zone. Dripwater Na^+ concentrations exhibit a statistically significant decreasing trend over the entire eight years of monitoring at each drip site (Supplemental Table S6 and Fig. 4). The trends of decreasing Na^+ concentrations over the study interval is consistent with (i) increasingly higher drip rates during subsequent dry seasons over the time interval of study at all the drip sites reflecting increased storage in the vadose zone (Fig. 4), and (ii) increasing precipitation amounts over the time interval of study driving dilution of Na^+ concentrations of water stored in the vadose zone by infiltrating meteoric water (Figs. 4 and 6).

$\delta^{18}O_{precip}$ values exhibit prominent seasonal variability, with lower values during wetter months (Supplemental Fig. S2). Temporal variability in $\delta^{18}O_{precip}$ is greater relative to that observed in cave dripwater and groundwater (Fig. 6), likely reflecting homogenization of $\delta^{18}O_{precip}$ variability due to mixing in the vadose and phreatic zones. Mean dripwater and groundwater $\delta^{18}O$ values (−6.4‰ and −6.2‰, respectively) are lower than the weighted-mean value for $\delta^{18}O_{precip}$ (−5.4‰), indicating preferential recharge of rainwater with low $\delta^{18}O$ values. The mean precipitation-weighted $\delta^{18}O_{precip}$ value for the months of August to October is −6.3‰. Assuming that the groundwater isotopic composition is the amount-weighted average of rainwater that actually recharges the system, this indicates that recharge may be predominately during the wet season and is a result consistent with previous work on Guam (Jocson et al., 2002; Jones and Banner, 2003; Partin et al., 2011) and other tropical carbonate islands (Jones and Banner, 2003). Further, preferential recharge during the wet season is consistent with the conceptual model in which water recharging the cave, likely during the wet season, has not experienced significant evaporation, but is carrying with it dissolved salts from the evaporation of previous rainfall, likely during the dry season, that did not recharge the cave.

Cave dripwater $\delta^{18}O$ values exhibit an observable decreasing trend during the last one to two years at each site, with a statistically significant (p-value < 0.001, Supplemental Table S6) decrease in three of the four sites. These trends occur despite the absence of a significant trend in precipitation $\delta^{18}O$ values or annual precipitation-weighted mean values of $\delta^{18}O_{precip}$ from recharge months (i.e., August, September, and October) (Fig. 6). The nature of rainfall, however, is notably different before and after the 2013 wet season, with higher cumulative monthly rainfall totals during dry and wet seasons following the 2013 wet season (Fig. 6). More-intense precipitation may promote

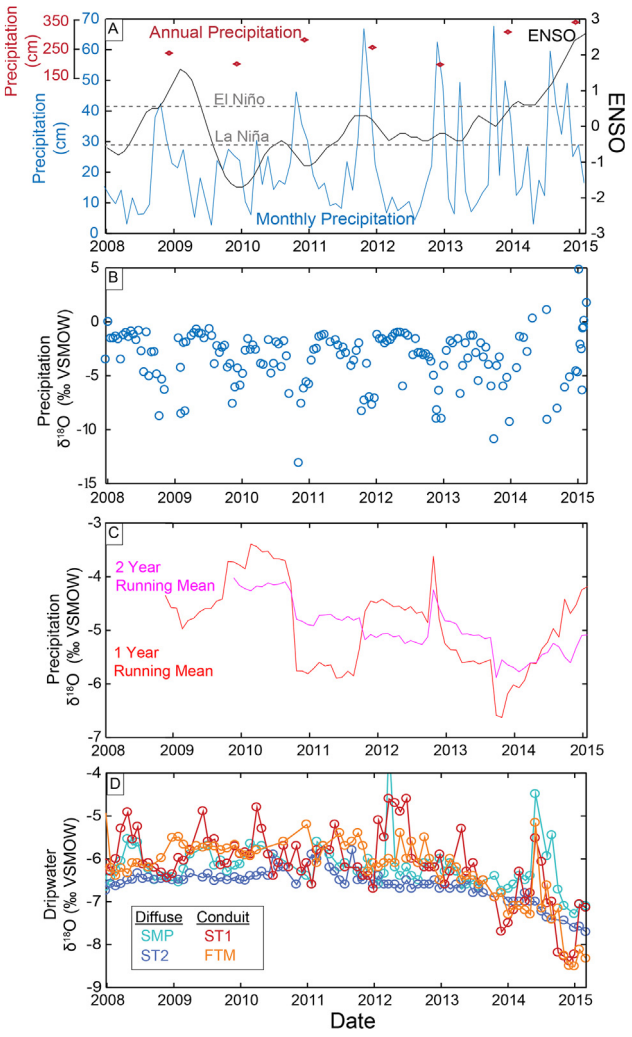

Fig. 6. (A) Time series of monthly (blue) and annual (red) cumulative precipitation for Guam with the El Niño Southern Oscillation 3.4 index (black). (B) Bi-weekly $\delta^{18}O_{precip}$ values. (C) One- and two-year running mean for annual precipitation-weighted $\delta^{18}O_{precip}$ values during the recharge months (i.e. August, September, and October). (D) Monthly cave dripwater $\delta^{18}O$ values. (For interpretation of the references to color in this figure legend, the reader is referred to the web version of this article.)

greater runoff and enhance the recharge bias toward isotopically lighter precipitation (Jones and Banner, 2003). Furthermore, a marked decrease in the extent to which drip rates decline over the dry season indicate that such changes in precipitation amount translate to increased recharge and water in vadose zone storage.

Cave dripwater $\delta^{18}O$ values are slightly more variable at fracture-supplied sites relative to diffuse-supplied sites (Fig. 7), and $\delta^{18}O$ values at diffuse-supplied sites are slightly lower relative to fracture-supplied sites. These results are consistent with the flow paths along dissolution enhanced fracture networks facilitating more direct infiltration of water relative to diffuse flow paths, leading to greater reflection of the isotopic variability occurring in $\delta^{18}O_{precip}$ values and less of a recharge bias. That is, the difference in mean values between sites supplied by fracture vs diffuse flow paths (Fig. 7B and C) reflects differences in the sensitivity of these flow paths to changes in hydrologic conditions at the surface.

5. Conclusions

Analysis of the spatial and temporal variability of geochemical and isotopic compositions of cave dripwater and groundwater over an

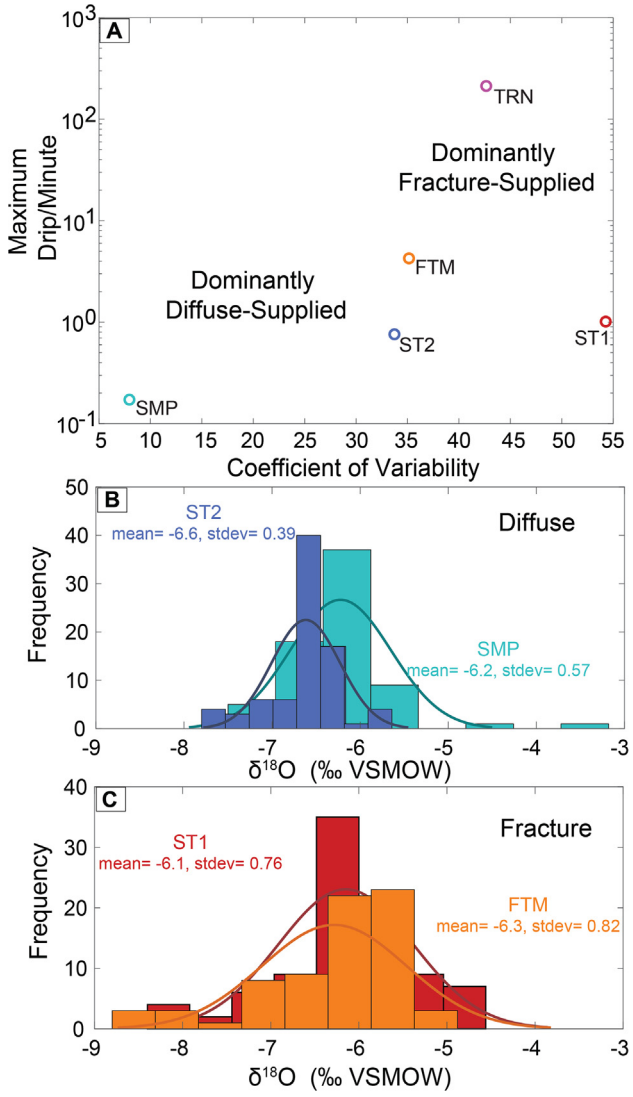

Fig. 7. (A) Drip-site categorization based on maximum drip rate and coefficient of variability. (B and C) $\delta^{18}O$ distribution for dominantly diffuse- and fracture-supplied dripwater sites, respectively.

interval that spanned a transition from dry to wet conditions independently reinforces the existing conceptual model of recharge and groundwater flow in the NGLA. This model, up to now, has been based mainly on observations of physical hydrogeology, unconditioned by geochemical observations. Specifically, we find geochemical evidence that:

- The sensitivity of the freshwater lens to intra- and inter-annual changes in recharge is spatially variable, as evidenced by the geochemical variability observed in wells distributed across the study area (Figs. 1, 3, and 5).
- Groundwater compositions are influenced by water-rock interaction and mixing between recharging meteoric water and seawater (up to 1%), as evidenced by the ability of geochemical and isotope modeling to explain observed groundwater compositions (Figs. 3 and 5).
- Dissolution enhanced fracture networks constitute preferential recharge pathways, as evidenced by distinct geochemical and isotopic variability of fracture-supplied and diffuse-supplied sites (Figs. 4, 6, and 7).
- Recharge is sensitive to inter-annual changes in precipitation amount and intensity, as evidenced by intra- and inter-annual variations in the geochemical and isotopic compositions of groundwater (Figs. 4 and 6).
- Recharge predominantly occurs during the wet season based on the coincidence of average groundwater $\delta^{18}O$ values with the amount-weighted average $\delta^{18}O_{precip}$ values occurring during the wet season (Figs. S2 and 6).
- The freshwater lens is, isotopically and geochemically, buffered from the hydroclimatic variability that occurred during the study. This is supported by the limited variability in isotopic and geochemical compositions of both cave dripwater and groundwater relative to the magnitude of intra- and inter-annual variability in precipitation amount and precipitation isotopic compositions (Figs. 4 and 6).

Acknowledgements

We acknowledge support from the Strategic Environmental Research and Development Program (SERDP Project Number 13 RC01-004/RC-2340), and the Pacific Islands Climate Science Center (G12AC0003). This research was also supported by NSF EAR-1452024 to J. Gulley, D. Breecker, and J. Banner, NSF AGS-1003700 to J. Partin, J. Jenson, and J. Banner, and NSF AGS-1404003 to J. Partin.

Appendix A. Supplementary data

Supplementary data to this article can be found online at https://doi.org/10.1016/j.jhydrol.2018.10.049.

References

Australian Bureau of Meteorology & CSIRO, 2011. Climate change in the Pacific – Scientific assessment and new research: v. 1 Regional overview, v. 2.
Allen, M.R., Ingram, W.J., 2002. Constraints on future changes in climate and the hydrologic cycle. Nature 419, 224–232.
Banner, J.L., Musgrove, M., Edwards, R.L., Asmerom, Y., Hoff, J.A., 1996. High-resolution temporal record of Holocene ground-water chemistry: Tracing links between climate and hydrology. Geology 24, 1049–1052.
Banner, J.L., Hanson, G.N., 1990. Calculations of simultaneous isotopic and trace-element variations during water-rock interaction with applications to carbonate diagenesis. Geochim. Cosmochim. Acta 54, 3123–3137.
Bautista, K.K., Jenson, J.W., Lander, M.A., Righetti, T., 2018. Vadose Hydrology at Jinapsan Cave, Northern Guam. Technical Report #163. Water and Environmental Research Institute of the Western Pacific, University of Guam, Mangilao, Guam, pp. 130.
Chandrajith, R., Diyabalanage, S., Premathilake, K.M., Hanke, C., van Geldern, R., Barth, J.A.C., 2016. Controls of evaporative irrigation return flows in comparison to seawater intrusion in coastal karstic aquifers in northern Sri Lanka: evidence from solutes and stable isotopes. Sci. Total Environ. 548–549, 421–428. https://doi.org/10.1016/j.scitotenv.2016.01.050.
Contractor, D.N., Jenson, J.W., 2000. Simulated effect of vadose infiltration of water levels in the Northern Guam Lens Aquifer. J. Hydrol. 229, 232–254.
Eidvin, T., Ullmann, C.V., Dybkær, K., Rasmussen, E.S., Piasecki, S., 2014. Discrepancy between Sr isotope and biostratigraphic datings of the upper middle and upper Miocene successions (Eastern North Sea Basin, Denmark). Palaeogeogr. Palaeoclimatol. Palaeoecol. 411, 267–280.
ESRI, GEBCO, NOAA, National Geographic, DeLorme, HERE, Geonames.org, et al., 2017. Ocean Basemap, imagery accessed via ArcGIS July, 2017.
Gingerich, S.B., 2003. Hydrologic Resources of Guam, U.S. Geological Survey Water-Resources Investigations Report 03-4126, 2 Plates.
Gingerich, S.B., 2013. The effects of withdrawals and drought on groundwater availability in the Northern Guam Lens Aquifer, Guam, U.S. Geological Survey Scientific Investigations Report 2013-5216, available at https://pubs.er.usgs.gov/publication/sir20135216.
Guard, C.P., Hamnett, M.P., Neumann, C.J., Lander, M.A., Jenson, J.W., 2009. Vadose flow synthesis for the Northern Guam Lens Aquifer. Technical Report #85. Water and Environmental Research Institute of the Western Pacific, University of Guam, pp. 156.
Hickey-Vargas, R., Reagan, M.K., 1987. Temporal variation of isotope and rare earth element abundance in volcanic rocks from Guam: implications for the evolution of the Mariana Arc. Contrib. Miner. Petrol. 97, 497–508.
Hodell, D.A., Mueller, P.A., Garrido, J.R., 1991. Variations in the strontium isotopic compositions of seawater during the Neogene. Geology 19, 24–27.
IAEA/WMO, 2018. Global Network of Isotopes in Precipitation. The GNIP Database Accessible at: http://www.iaea.org/water.
Jenson, J.W., Keel, T.M., Mylroie, J.R., Mylroie, J.E. Stafford, K.W., Taborosi, D., Wexel, C., 2006, Karst of the Mariana Islands: The interaction of tectonics, glacio-eustasy, and fresh/sweater mixing in island carbonates, Geological Society of America Special Papers, Perspectives on Karst Geomorphology, Hydrology, and Geochemistry – A

Tribute Volume to Derek C. Ford and William B. White 404, pp. 129–138.
Jones, I.C., Banner, J.L., 2003. Estimating recharge thresholds in tropical karst island aquifers, Barbados, Puerto Rico and Guam. J. Hydrol. 278, 131–143.
Jocson, J.M.U., Jenson, J.W., Contractor, D.N., 2002. Recharge and aquifer response: northern Guam Lens Aquifer, Guam, Mariana Islands. J. Hydrol. 260 (1–4), 231–254.
Johnson, A.G., 2012. A water-budget model and estimates of groundwater recharge for Guam, U.S. Geological Survey Scientific Investigations Report 2012-5028, available at http://pubs.usgs.gov/sir/2012/5028/.
Kossin, J.P., Emanual, K.A., Camargo, S.J., 2016. Past and projected changes in Western North Pacific Tropical Cyclone Exposure. J. Clim. 29, 5725–5739.
Lander, M.A., 1994a. Meteorological Factors Associated with Drought on Guam: Water and Environmental Research Institute of the Western Pacific. University of Guam Technical Report no. 75, 39 p.
Lander, M.A., 1994b. An exploratory analysis of the relationship between tropical storm formation in the Western North Pacific and ENSO. Am. Meteorol. Soc. 122, 636–651.
McArthur, J.M., Rio, D., Massari, F., Castradori, D., Bailey, T.R., Thirlwall, M., Houghton, S., 2006. A revised Pliocene record for marine- 87Sr/86Sr used to date an interglacial event recorded in the Cockburn Island Formation, Antarctic Peninsula. Palaeogeography, Palaeoclimatology, Palaeoecology 242, 126–136.
Mink, J.F., Vacher, H.I., 1997. Hydrogeology of northern Guam. Geol. Hydrogeol. Carbonate Islands 743–761.
Mahler, B.J., Garner, B.D., Musgrove, M., Guilfoyle, A.L., Rao, M.V., 2006. Recent (2003–2005) Water Quality of Barton Springs, Austin, Texas, with Emphasis on Factors Affecting Variability. U.S. Geological Survey Scientific Investigations Report 2006–5299, 83 p.
Moerman, J.W., Cobb, K.M., Partin, J.W., Meckler, A.N., Carolin, S.A., Adkins, J.F., Lejau, S.L., Maland, J., Clark, B., Tuen, A.A., 2014. Transformation of ENSO-related rainwater to dripwater $\delta^{18}O$ variability by vadose water mixing. Geophys. Res. Lett. 41, 7907–7915.
Musgrove, M., Banner, J.L., 2004. Spatial and temporal variability of vadose dripwater geochemistry: Edwards Aquifer, central Texas. Geochimica et Coscochimica Acta 68, 1007–1020.
Mylroie, J.E., Jenson, J.W., 2000. CIKM, the carbonate island karst model. Geological Society of America Abstracts with Programs, pp. A-355.
Mylroie, J.E., Jenson, J.W., Taborosi, D., Jocson, J.M.U., Vann, D.T., Wexel, C., 2001. Karst features on Guam in terms of general model of carbonate island karst. J. Cave Karst Stud. 63, 9–22.
Noronha, A.L., Hardt, B.F., Banner, J.L., Jenson, J.W., Partin, J.W., James, E.W., Lander, M.A., Bautista, K.K., 2016. Trade winds drive pronounced seasonality in carbonate chemistry in a tropical Western Pacific island cave—Implications for speleothem paleoclimatology. Geochem. Geophys. Geosyst org/10.1002/2016GC006644.
Park, D.-S.R., Ho, C.-H, Chan, J.C.L., Ha, K.-J., Kim, H.-S, Kim, J., Kim, J.-H., 2017. Asymmetric response of tropical cyclone activity to global warming over the North Atlantic and western North Pacific from CMIP5 model projections 7, 41351, 10.1038/srep41354.
Partin, J.W., Jenson, J.W., Banner, J.L., Quinn, T.M., Taylor, F.W., Sinclair, D., Hardt, B., Lander, M.A., Bell, T., Miklavič, B., Jocson, J.M.U., Taboroši, 2011. Relationship between modern rainfall variability, cave dripwater and stalagmite geochemistry in Guam, USA. Geochem. Geophys. Geosyst. 13, Q03013. https://doi.org/10.1029/2011GC003930.
Rotzoll, Kolja, Gingerich, S.B., Jenson, J.W., El-Kadi, A.I., 2013. Estimating hydraulic properties from tidal attenuation in the Northern Guam Lens Aquifer, territory of Guam. Hydrogeol. J. 21 (3), 643–654.
Tracey, J.I., Jr., Schlanger, S.O., Stark, J.T., Doan, D.B., May, H.G., 1964. General Geology of Guam, 403-A. U.S. Geological Survey Professional Paper.
Schlanger, S.O., 1964, Petrology of the limestones of Guam. Geologic Survey Professional Paper 403-D.
Schwarz, K., Barth, J.A.C., Postigo-Rebollo, C., Grathwohl, P., 2009. Mixing and transport of water in a karst catchment: a case study from precipitation via seepage to the spring. Hydrol. Earth Syst. Sci. 13 (3), 285–292.
SEIS (Supplemental Environmental Impact Statement), 2018. Guam and CNMI Military Relocation; Relocating Marines from Okinawa, Japan to Guam, https://Guambuildupeis.us, accessed 27 Apr 2018.
Sinclair, D.J., Banner, J.L., Taylor, F.W., Partin, J., Jenson, J., Mylroie, J., Goddard, E., Quinn, T., Jocson, J., Miklavic, B., 2012. Magnesium and strontium systematics in tropical speleothems from the Western Pacific. Chem. Geol. 294-5, 1–17.
Turekian, 1968. Oceans, Foundations of earth science series. Prentice-Hall, Englewood, Cliffs, N.J, pp. 120.
U.S. Census Bureau, 2011. Table 1313. Estimated resident population with projections: Statistical Abstract of the United States; 2010, Puerto Rice and the Island Areas, http://www.census.gov/compendia/statab/cats/puerto_rico_the_island_areas.html.
Vacher, H.L., Mylroie, J.E., 2002. Eogenetic karst from the perspective of an equivalent porous medium. Carbonate Evaporites 17 (2), 182–196.
Vann, D.T., Bendixson, V.M., Roff, D.F., Simard, C.A., Schumann, R.M., Habana, N.C., Jenson, J.W., 2014. Topography of the Basement Rock Beneath the Northern Guam Lens Aquifer and its Implications for Groundwater Exploration and Development. Technical Report #142. Water and Energy Research Institute of the Western Pacific, pp. 90.
Vörösmarty, C.J., Pamela, G., Salisbury, J., Lammers, R.B., 2000. Global water resources: vulnerability from climate change and population growth. Science 298 (5477), 284–288.
Ward, P.E., Hoffard, S.H., Davis, D.A., 1965. Hydrology of Guam, U.S. Geological Survey, Professional Paper 403-H.
Water and Environmental Research Institute of the Western Pacific and Island Research and Education Initiative, 2017. Digital Atlas of Northern Guam, Northern Guam geospatial information server, accessed July, 2017, available at http://north.hydroguam.net/gis_download.php.
Widlansky, M.J., Annamalai, H., Gingerich, S.B., Storlazzi, C.D., Marra, J.J., Hodges, K.J., Choy, B., Kitoh, A., 2018. Tropical cyclone projections: changing climate threats for Pacific Island defense installation. Clim. Soc. Weather in press.
Wortham, B.E., Wong, C.I., Silva, L.C.R., McGee, D., Montañez, P., Rasbury, E.T., Cooper, K.M., Sharp, W.D., Glessner, J.J.G., Santos, R.V., 2017. Assessing response of local moisture conditions in central Brazil to variability in regional monsoon intensity using speleothem $^{87}Sr/^{86}Sr$ values. Sci. Lett in press.
Wong, C.I., Banner, J.L., Musgrove, M., 2011. Seasonal dripwater Mg/Ca and Sr/Ca variations driven by cave ventilation: implications for and modeling of speleothem paleoclimate records. Geochim. Cosmochim. Acta 75, 3514–3529.
Wong, C.I., Mahler, B.J., Musgrove, M., Banner, J.L., 2012. Changes in sources and storage in a karst aquifer during a transition from drought to wet conditions. J. Hydrol. 468–469, 159–172.